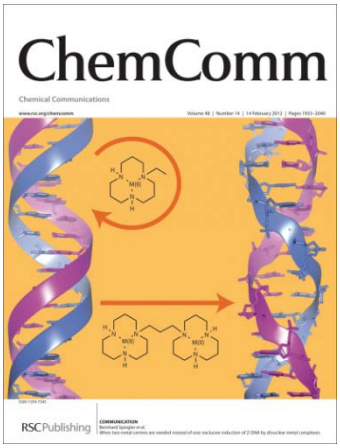

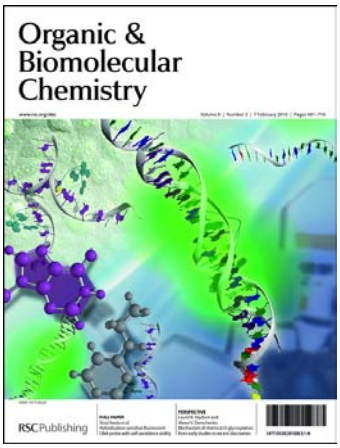

This article is part of the

Nucleic acids: new life, new materials

web-themed issue

Guest edited by:

Mike Gait Medical Research Council, Cambridge, UK	**Ned Seeman** New York University, USA	**David Liu** Harvard University, USA	**Oliver Seitz** Humboldt-Universität zu Berlin, Germany	**Makoto Komiyama** University of Tsukuba, Japan	**Jason Micklefield** University of Manchester, UK

All articles in this issue will be gathered online at

www.rsc.org/nucleic_acids

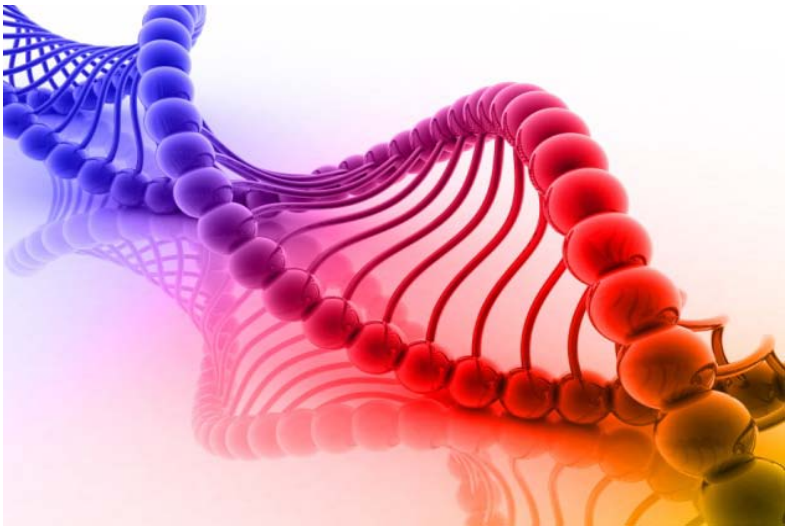

Organic & Biomolecular Chemistry

Dynamic Article Links

Cite this: *Org. Biomol. Chem.*, 2012, **10**, 6537

www.rsc.org/obc

PAPER

Pyridostatin analogues promote telomere dysfunction and long-term growth inhibition in human cancer cells†

Sebastian Müller,[a] Deborah A. Sanders,[a] Marco Di Antonio,[a] Stephanos Matsis,[a] Jean-François Riou,[b] Raphaël Rodriguez[a] and Shankar Balasubramanian[a,c,d]

Received 1st May 2012, Accepted 21st June 2012
DOI: 10.1039/c2ob25830g

The synthesis, biophysical and biological evaluation of a series of G-quadruplex interacting small molecules based on a *N*,*N*′-bis(quinolinyl)pyridine-2,6-dicarboxamide scaffold is described. The synthetic analogues were evaluated for their ability to stabilize telomeric G-quadruplex DNA, some of which showed very high stabilization potential associated with high selectivity over double-stranded DNA. The compounds exhibited growth arrest of cancer cells with detectable selectivity over normal cells. Long-time growth arrest was accompanied by senescence, where telomeric dysfunction is a predominant mechanism together with the accumulation of restricted DNA damage sites in the genome. Our data emphasize the potential of a senescence-mediated anticancer therapy through the use of G-quadruplex targeting small molecules based on the molecular framework of pyridostatin.

Introduction

Nucleic acids can adopt various non-Watson–Crick secondary structures including G-quadruplexes, a supramolecular architecture that can arise from certain G-rich sequences. Such structures comprise Hoogsteen hydrogen bonded guanines leading to the formation of G-quartets that stack *via* π–π interactions. The relative orientation of the strands and loop configurations can vary, giving rise to polymorphic conformations that can depend on the primary nucleic acid sequence, temperature, solvent and salt composition.[1–4]

There has been experimental data in support of G-quadruplex formation in the genomic DNA of several organisms.[5–8] Lipps, Rhodes and co-workers provided the first strong evidence for their existence in the ciliate *Stylonychia*. In their report, the authors demonstrated that folding into these motifs at the telomeric region of chromosomes is regulated by the Telomere End Binding Proteins (TEBP) α and β in a cell cycle-dependent manner, and might act as telomere capping structures.[9] Human telomeres comprise a highly repetitive G-rich DNA repeat sequence $(TTAGGG)_n$ [10] and the human telomeric G-quadruplex has been extensively studied *in vitro*.[11,12] It has been postulated that these motifs affect telomere elongation,[13] capping[14] and replication *in vivo*.[15] The production of telomeric repeat-containing RNA (TERRA) may also suggest a role during transcription.[16] In a seminal paper, Zahler *et al.* showed that certain G-rich telomeric sequences can form G-quadruplexes *in vitro*, rendering them resistant to extension by the reverse transcriptase telomerase.[17] Successive rounds of replication leads to progressive telomere shortening in normal cells, an event that is alleviated by telomerase conferring infinite proliferative capacity in ~85% of cancer cells.[18] These findings prompted us to design selective G-quadruplex interacting small molecules with the aim to develop a novel telomere based anticancer therapy.[19] However, recent reports have suggested that such molecules can induce telomere dysfunction in a telomerase independent manner.[14,20,21]

Telomeres comprise a protein complex named shelterin,[22] which covers and protects the ends of telomeres from the DNA-damage response machinery that promote non-homologous end-joining and homologous recombination. Small molecules interacting with G-quadruplexes have been shown to induce telomere dysfunctions by competing for binding with the shelterin components Telomeric Repeat Factor 1 (TRF1), Telomeric Repeat Factor 2 (TRF2) and Protection of Telomeres 1 (POT1), leading to progressive telomere shortening, anaphase bridges and aberrant chromosome segregation.[14,15,23] In addition, dysfunctional telomeres have been shown to activate the DNA damage response, resulting in cell cycle checkpoint activation and growth arrest.[24] Several putative G-quadruplex sequences, besides the telomeric repeat, have been identified in the human

[a]*Department of Chemistry, University of Cambridge, Lensfield Road, Cambridge, CB2 1EW, UK. E-mail: rr324@cam.ac.uk, sb10031@cam.ac.uk; Tel: +44 (0)1223 336347*
[b]*Regulation et Dynamique des Genomes, Museum National d'Histoire Naturelle, INSERM U565, CNRS UMR 7196, Paris, France*
[c]*Cancer Research UK, Cambridge Research Institute, Li Ka Shing Center, Cambridge, CB2 0RE, UK*
[d]*School of Clinical Medicine, University of Cambridge, Cambridge, CB2 0SP, UK*

†Electronic supplementary information (ESI) available: Experimental procedures and characterization of building blocks and pyridostatin analogues and FRET-melting profiles. See DOI: 10.1039/c2ob25830g

genome[25] with an enrichment in promoter regions of several proto-oncogenes[26] such as *c-kit*,[27,28] *c-myc*,[29,30] *bcl-2*[31] and *K-ras*.[32] Small molecules have been proposed to interact with promoter quadruplexes and to alter the expression of those genes *in cellulo*.[29,30,33,34] These motifs have also been identified in RNA[35–37] where they might have a functional role by modulating translation[21,38] and alternative splicing.[39] Further evidence for the existence of G-quadruplex motifs in human cells has been provided by recent work from Gibbons and co-workers, demonstrating that the alpha thalassemia/mental retardation syndrome X-linked (ATRX) helicase binds to clusters of G-quadruplex motifs, hence modulating the expression of these genes.[40]

Numerous studies on synthetic molecules that interact with G-quadruplexes have helped demonstrate the existence and elucidate putative biological roles of these nucleic acid structures.[41–50] Previously reported quinoline-based molecules selectively recognize G-quadruplex structures over double-stranded DNA with high potency, making this chemical moiety an attractive feature to exploit for the design of G-quadruplex ligands.[51–54] We previously reported a G-quadruplex stabilizing synthetic small molecule, based on a *N*,*N*′-bis(quinolinyl)pyridine-2,6-dicarboxamide scaffold (Fig. 1), which we named pyridostatin (**1**). We demonstrated the suitability of the molecule to target telomeres in cells.[23] The design of these molecules was initially based on structural features shared by a potent G-quadruplex binding molecule[54] with particular emphasis on (1) the ability to adopt a flat but flexible conformation, facilitated by an internal hydrogen bonding network, prone to adapt to the dynamic and polymorphic nature of diverse G-quadruplex structures; (2) an optimal electronic density of the aromatic surface to enable π–π interactions with the G-tetrad tuned by substituents (for instance alkoxy or halogens capable of altering the electron density) and (3) the presence of free nitrogen lone pairs able to coordinate with a molecule of water[55] or alternatively to sequester a monovalent potassium cation in the centre, thus locking the flat surface of the molecule and facilitating the interaction with G-quartets (Fig. 1). These key features distinguish pyridostatin from other structurally related G-quadruplex interacting molecules.[51–54] Prior to this work, we showed that pyridostatin, the lead compound of this family, induces telomere dysfunction by competing for binding with telomere associated proteins such as human POT1.[23] Furthermore, we have illustrated the ability of a biotinylated analogue to mediate the selective pull-down of telomeric fragments from genomic DNA by means of affinity matrix isolation. During the course of this study, we have demonstrated the high selectivity of pyridostatin analogues towards G-quadruplex nucleic acids, regardless of sequence variability and structure polymorphism, compared to double-stranded DNA.[56] Recent work in our laboratory has proven that pyridostatin alters transcription and replication of particular human genomic *loci* containing high G-quadruplex clustering within the coding region, which encompasses telomeres[57] and selected genes such as the proto-oncogene *SRC*.[58] These results emphasize that selective G-quadruplex ligands represent a new class of DNA damaging agents with limited sites of action throughout the genome, in contrast to well-known therapeutic agents previously reported to inducing genome-wide DNA damage in a stochastic manner associated with high cytotoxicity.

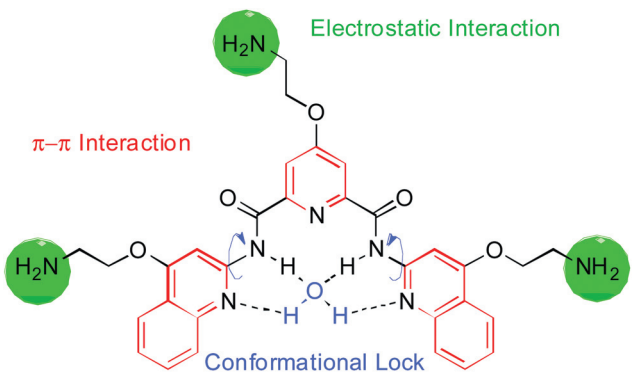

1

Fig. 1 Molecular structure of pyridostatin (**1**). The design rationale is indicated on the structure.

These results prompted us to synthesize structural variants based on the *N*,*N*′-bis(quinolinyl)pyridine-2,6-dicarboxamide scaffold to further explore the scope of their use as anti-cancer agents. We have used this family of compounds by keeping the central scaffold of pyridostatin intact and varying the substituents, including different cationic, neutral and glycosidic side-chains. These groups were systematically altered to gain further insights into structure–activity relationships. Herein, we describe an assessment of their potential to stabilize the telomeric G-quadruplex (H-Telo) and a selection of genomic promoter quadruplexes using a Förster Resonance Energy Transfer (FRET)-melting assay initially introduced by Mergny and Maurizot.[59] Furthermore, we have measured their growth inhibitory properties against a panel of human cancer cell lines as a first potency readout, and finally have explored the phenotype induced at telomeres.

Results

Chemical synthesis of pyridostatin analogues

In this study, 26 small molecules based on the *N*,*N*′-bis(quinolinyl)pyridine-2,6-dicarboxamide scaffold were synthesized in two to seven synthetic steps as shown in Schemes 1 and 2. We chose to systematically vary side chain lengths and their chemical functionalities, keeping the central scaffold of pyridostatin unaltered. Synthetic analogues were obtained by coupling one mole equivalent of pyridine-based building blocks with two mole equivalents of quinoline-based building blocks as depicted in Scheme 1. The central core was synthesized either from chelidamic acid (**2**) or the commercially available pyridine-2,6-dicarbonyl dichloride (**3**). Compounds **4a** and **4c** were prepared by reacting **2** with thionyl chloride followed by quenching the reaction mixture with cold methanol (MeOH). The products were separated by aqueous work-up yielding 29% of **4a** and 28% of **4c**. Compound **4b** was prepared in 90% yield from **2** in toluene–MeOH using (trimethylsilyl)diazomethane (Me_3SiCHN_2). Intermediate **4a** was further functionalized *via* a Mitsunobu reaction, mixing diisopropyl azodicarboxylate (DIAD) and triphenylphosphine in tetrahydrofuran (THF) at 0 °C then room temperature. The resulting 4-substituted 2,6-pyridine-dimethylesters were then deprotected in the presence of sodium hydroxide (NaOH) in

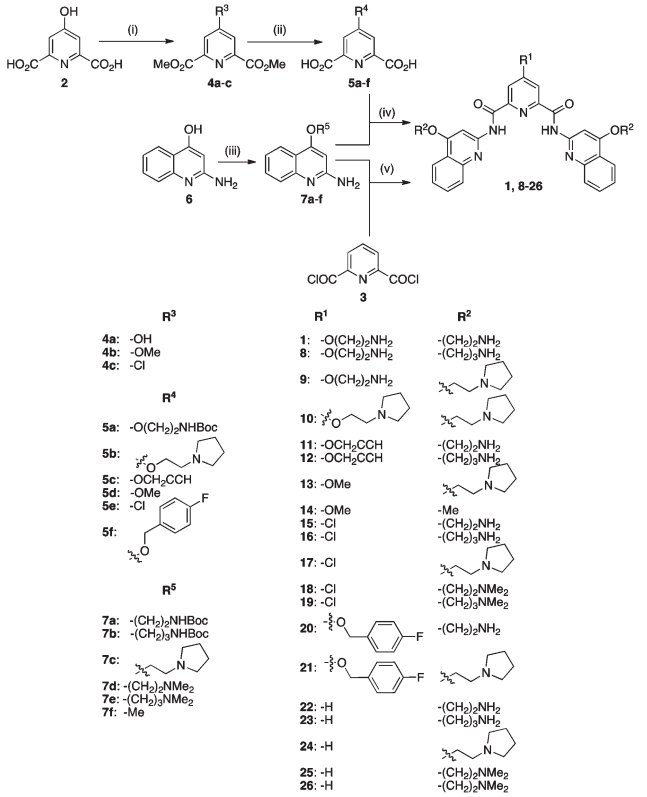

Scheme 1 Synthetic route to compounds **1** and **8–26**. (i) **4a**, **4c**: $SOCl_2$, MeOH, 0 °C then rt, 2 h; **4b**: toluene–MeOH, Me_3SiCHN_2, rt, 30 min; (ii) **5a–c**, **5f**: ROH, triphenylphosphine, DIAD, THF, 0 °C to rt, 3 d; then for **5a–f**: NaOH (aq.), MeOH, rt, 1 h; (iii) **7a–e**: ROH, triphenylphosphine, DIAD, THF, 0 °C to rt, 3 d; **7f**: toluene–MeOH, Me_3SiCHN_2, rt, 30 min; (iv) **1**, **8–21**: **5a–f**, 1-chloro-*N*,*N*,2-trimethylpropenyl-amine, DCM, 2 h, then triethylamine, 0 °C, 1 h then rt, then **7a–f**, overnight; then for **1**, **8**, **9**, **11**, **12**, **15**, **16**, **20**: TFA–DCM, rt, 1 h; (v) **22–26**: **2**, triethylamine, DCM, 0 °C, 1 h, then **7a–f** overnight; then for **22**, **23**: TFA–DCM, rt, 1 h.

H_2O–MeOH to afford the pyridine-based building blocks **5a–f** in 57–77% yield. The quinoline-based building blocks were obtained in 53–71% yield from commercially available starting material 2-amino-quinolinone (**6**) either *via* a similar Mitsunobu reaction to provide **7a–e**, or through a direct methylation in the presence of toluene–MeOH containing Me_3SiCHN_2. Building blocks **5a–f** were reacted with Ghosez's reagent (1-chloro-*N*,*N*,2-trimethylpropenyl-amine) and then with triethylamine, followed by the addition of **7a–f** to obtain products **1**, **8–21** in 61–93% yield. Compounds **8–9**, **11–12**, **15–16** and **20** were then deprotected using trifluoroacetic acid (TFA) in dichloromethane (DCM). Compound **3** was reacted with **7a–g** in the presence of triethylamine to provide compounds **22–26** in 62–82% yield. Finally, compounds **27–33** were synthesized in 22–67% yield from **11** and **12** using the copper catalyzed alkyne–azide 1,3-dipolar cycloaddition as shown in Scheme 2.

Compounds **31–33** were conveniently obtained with retention of configuration, in mild conditions and without the use of protecting groups, highlighting the flexibility of this protocol.[60] It is noteworthy that the condensed products of building blocks **5b**, **5d** and **5f** with **7a–b**, **7f** could be precipitated from hot acetonitrile (MeCN) yielding either the final molecule, or a Boc (di-

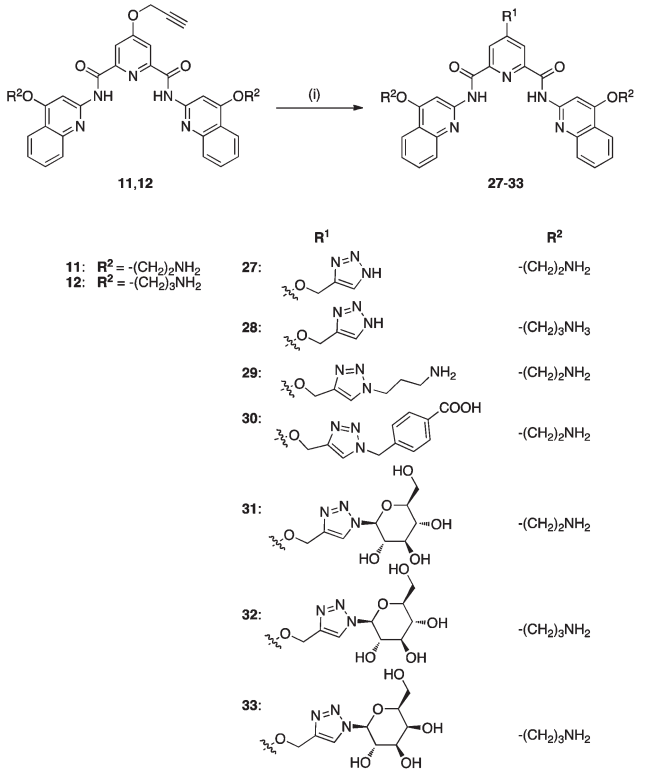

Scheme 2 Synthetic route to compounds **27–33**. (i) **27**, **29–31**: **11**, $CuSO_4{\cdot}5H_2O$, sodium L-ascorbate, RN_3, H_2O–^{t}BuOH, rt, overnight; **28**, **32**, **33**: **12**, $CuSO_4{\cdot}5H_20$, Sodium L-ascorbate, RN_3, H_2O–^{t}BuOH, rt, overnight.

tert-butyl dicarbonate)-protected derivative, avoiding chromatographic purification, which then afforded the target molecule using standard TFA deprotection in DCM. Final products **1**, **8–33** were further purified by high performance liquid chromatography (HPLC) to ensure high purity for the biophysical, *in vitro* and *in vivo* assays used in our subsequent studies. Molecules **22–26** all lack a side chain at position 4 of the pyridine ring, thus enabling us to investigate the relevance of that substitution for G-quadruplex stabilization and ensuing associated biological effects. Compounds **1**, **8–14** carry side chains with varying chemical functionalities on the pyridine core as well as the quinoline moiety, which may influence the recognition towards different quadruplexes and relative conformations. We also introduced a chlorine onto the pyridine core (**15–19**) as well as a side chain containing a fluorinated benzene ring (**20–21**), which have the potential to participate in interactions with G-quadruplex loops or change the electron density of the pyridine core, and may thus provide additional selectivity over duplex DNA (ds-DNA).[61] Compounds **27–33** were synthesized using the copper modified Huisgen reaction (Scheme 2), which enabled the introduction of complex functionalities such as sugar-containing asymmetric centers, capable of multiple hydrogen bond networking.

Biophysical evaluation of G-quadruplex stabilization by pyridostatin analogues

In order to study the interaction of the molecules with telomeric G-quadruplex DNA, we performed a Förster resonance energy

transfer (FRET)-melting assay[59] using the human telomeric G-quadruplex-forming sequence (H-Telo) and a ds-DNA as targets. The data are described in Table S1.† A large number of molecules of this family showed up to 35 K stabilization of H-Telo at 1 μM in melting experiments. None of the molecules studied showed any detectable stabilization of ds-DNA at this concentration, demonstrating the suitability of the scaffold for cell-based assays. Molecules **1**, **8–10**, which contain multiple amine functionalities, exhibited maximal stabilization for H-Telo at 1 μM ligand (Fig. 2, Table S1†).

Similarly, introducing other functions at position 4 of the pyridine moiety such as a chlorine (compounds **15–19**) or sugars (compounds **31–33**) improved the stabilization properties of the named compounds towards H-Telo compared to the unsubstituted analogues. This data set suggests that cation–dipole interactions as well as hydrogen and halogen-bonding interactions enable the improvement of the binding properties of the main scaffold towards G-quadruplex motifs. Conversely, removal of amine functionalities at positions R^1 and R^2, as for compounds **13–14**, was found to reduce the stabilizing potential of the corresponding scaffold, thus further demonstrating the need for polar functionalities to promote G-quadruplex stabilization. Ligands carrying an alkyne functionality (**11–12**) induced moderate ΔT_m-values, most likely due to the lack of the above mentioned stabilizing interactions. Ligands **27–29** also showed moderate stabilization of H-Telo, which was rather surprising for compound **29**, since this analogue contains three positively charged functionalities that have been shown to be stability-enhancers for all the other members of this family. Additionally, the introduction of a negatively charged functionality to afford **30** hampered the ability of this analogue to interact with H-Telo, presumably due to electrostatic repulsion with the negatively charged phosphate backbone of the DNA. The 4-fluorobenzyloxy substitution at position R^1 of ligands **20** and **21** resulted in lower ΔT_m values of 8.8 K and 4.3 K, respectively. These results are consistent with those observed for alkyne substituted analogues and suggest that the steric hindrance imposed by the benzene and triazole rings at the central position may lead to a weaker contribution of the fluorine and amine substituents. However, this is not the case for compounds **31–33**, since the sugar moieties might be involved in stabilizing non-covalent interactions, raising the ΔT_m-values recorded for these compounds to above 30 K. The nature of the amine on the side chain at position R^2 was found to have a small influence on the stabilization potential of the analogues following the general trend: $-NMe_2 \geq -NH_2 \geq$ –pyrrolidine. Comparing ΔT_m-values for **1** and **8**, **15–16**, **18–19**, **22–23**, **25–28** and **31–32**, respectively, showed that a three-carbon side chain gives slightly higher stabilization potentials than two-carbon side chains. Finally, we have investigated the selectivity of each molecule for G-quadruplex over ds-DNA by measuring the melting of H-Telo in the presence of increasing amounts of each analogue and 50 mole equivalents of unlabelled ds-DNA competitor. Negligible changes in melting temperatures were observed, further demonstrating a high specificity of these compounds for quadruplex DNA over ds-DNA, as was shown before for this type of scaffold[23,56] (see Fig. 2). Encouraged by these results, we next evaluated the stabilization properties of these compounds over various G4 structures before studying their aptitude to induce a phenotype in cell-based assays (see Fig. 3).

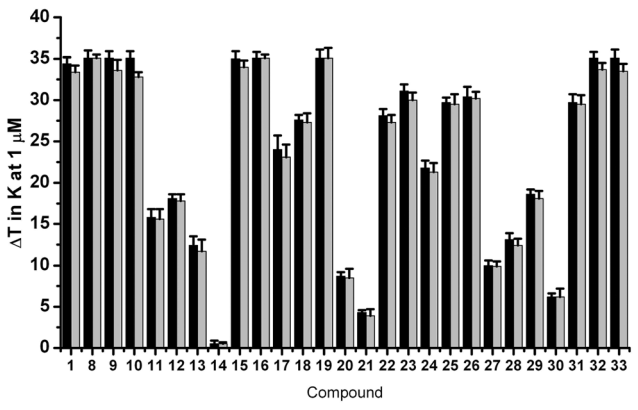

Fig. 2 FRET-melting competition results at 1 μM for **1**, **8–33** in the presence of 50 mol. equiv. of unlabeled ds-DNA against H-Telo. Values are expressed as ΔT_m. Black: ΔT_m in the absence of ds-DNA. Grey: ΔT_m in the presence of ds-DNA. Errors denote the standard deviation of at least three independent experiments.

Evaluation of cell viability upon exposure to analogues of pyridostatin

The molecules were assessed for their ability to inhibit cell growth using a luminescent cell viability assay. We investigated growth inhibition after 3 days of exposure to compounds **1**, **8–33** on a panel of four human cell lines: HeLa (adenocarcinoma), HT1080 (fibrosarcoma), U2OS (osteosarcoma), and WI-38 (normal lung fibroblasts), the latter being non-cancerous. The data are summarized in Fig. 3 and Table S2.† Molecules **1**, **9–10**, **15–19** and **22–26** showed growth inhibition at high nanomolar to low micromolar concentrations against the panel of

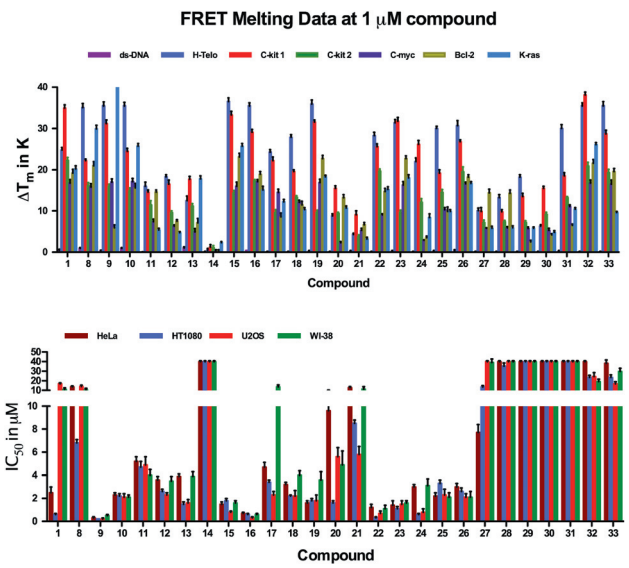

Fig. 3 Representation of FRET melting values for various G-quadruplex structures (*top*) and IC_{50}-values of growth inhibition after 72 h (*bottom*) treatment with compounds **1**, **8–33**. Errors denote the standard deviation of at least three independent experiments.

cell lines. Compound **9** displayed the lowest values of the series with IC_{50}-values ranging from 0.2 to 0.5 μM. This suggests that positively charged side chains may be required for improving the water solubility and cellular uptake of the apolar central skeleton, in addition to participating in favorable non-covalent interactions with the DNA targets. It is noteworthy that most of the compounds showed generally lower IC_{50}-values for the cancer cell lines than for the normal cell line WI-38. For example, pyridostatin (**1**) exhibited an 18.5-fold selectivity for HT1080 cells over WI-38 cells. Analogues **17** and **27** were found to be the most selective molecules for HeLa and U2OS with a 6.0- and 5.2-fold difference in growth inhibition over WI-38 cells, respectively. Notably, compounds **27–33**, which contain a triazole at position R^1, showed relatively higher IC_{50}-values as compared to other analogues, which might reflect differences in cell permeability and uptake of these analogues, since the sugar functionalized compound retained remarkable stabilization properties. Ligand **14**, which contains no functionalities, did not exhibit growth inhibitory properties at the concentrations used, thus reflecting on the poor solubility properties of this analogue and weak G-quadruplex stabilization potential. These results are in agreement with our previous reports[23,58] showing that this family of small molecules promotes DNA double strand break formation, which results in cell cycle arrest and growth inhibition.

Long-term growth inhibitory effects of pyridostatin analogues towards HT1080 cells

We investigated the long-term growth effects on HT1080 cells of a selection of molecules, namely **1**, **9–10**, **15–17**, **19–24**, **26–27** and **33**, by incubating cells over a period of 30 days with the compounds (Fig. 4) at their respective IC_{50}-values. Some of the molecules caused a strong reduction of population doublings indicating a long-term growth arrest of HT1080 cells, notably **1**, **15** and **17** after 6 days, **9** after 12 days and **10** and **21** after 21 days of exposure. Compounds **20** and **33** also caused a decrease in population doublings over time, with a flattening of the curve starting after 19 and 25 days of exposure, respectively.

Compounds **16**, **19**, **22–24**, **26** and **27** did not show any additional decrease in population doublings over the time-course measured, as compared to what would be expected for incubation at the IC_{50}. No change of population doublings was observed over the time course measured for compounds that did not have a substitution at position 4 of the pyridine ring (compounds **22–26**). It is worth noting that 97–99% of the control and the cells treated at the respective IC_{50}-value of each compound (**1**, **9–10**, **15–17**, **19–24**, **26–27** and **33**) were viable during the long-term treatment as observed by trypan blue nuclear exclusion, indicative of growth arrest as opposed to cytotoxicity induced by this family of compounds. In addition, the total cell number reached a plateau after long-term exposure without noticeable decrease, which also supports the absence of major cell killing. Our results indicate that complex mechanisms of action for these compounds are taking place. One of these mechanisms may involve the induction of dysfunctional telomeres, as previously shown for **1**, due to a competition for binding of these analogues with telomere binding proteins and ensuing telomere shortening. To verify this hypothesis we investigated the influence of these analogues on telomere G-overhang integrity in HT1080 cells.

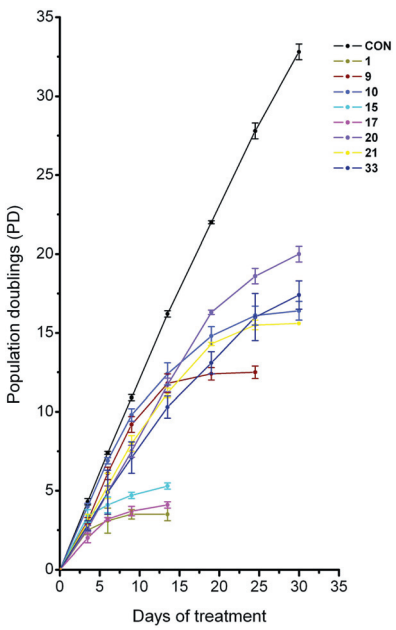

Fig. 4 Studies of long-term growth effect of compounds **1**, **9**, **10**, **15**, **17**, **20**, **21** and **33** on HT1080 cells. CON denotes control cells, which were not treated with compound. Measurements were taken at the respective IC_{50} values of the compounds.

G-overhang shortening and cellular senescence induced by analogues of pyridostatin

Small molecules that can compete for binding with shelterin components have been shown to induce telomere shortening, G-overhang degradation and replicative senescence in cultured cells.[23,47,56,62] We chose compounds **9–10**, **15**, **17** and **33**, since these analogues displayed moderate to high stabilization of the telomeric G-quadruplex H-Telo as judged by FRET-melting assays and long-term growth arrest occurring between 6 to 25 days of treatment. A β-galactosidase assay performed on HT1080 cells after 8 days of incubation with compounds **9–10**, **15**, **17** and **33** at their respective IC_{50} revealed the presence of senescent cells (Fig. S4†). No senescent cells were observed in mock treated cells.

We decided to measure telomere G-overhang lengths after treatment by employing a non-denaturing hybridization assay.[62] The experiments were performed using a 21C oligonucleotide (5′-$(CCCTAA)_3$CCC-3′) complementary to the 3′-G-overhang. G-overhang signals were assessed over a time course of 12 days, at five time-points (0 d, 3 d, 6 d, 9 d and 12 d). We found that all five analogues induced a decrease in the hybridization signal as compared to total genomic DNA stained with ethidium bromide (EtBr, Fig. 5). Consistent with a selective effect induced by the compounds, mock treated cells did not show any noticeable change in the hybridization signal. This showed that the telomeric G-overhang decreased in length over the time-course upon exposure to the small molecules. Interestingly, the kinetics

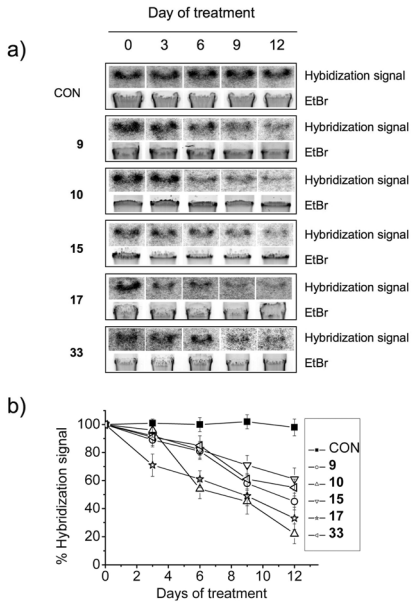

Fig. 5 Telomeric G-overhang shortening assessed for **9**, **10**, **15**, **17** and **33** in HT1080 cells by non-denaturing hybridization assay. CON represents DNA from cells grown in the absence of compound. Cells were incubated at the respective IC_{50} concentrations. (a) Hybridization gel radiograph and EtBr fluorescence picture. (b) Graph showing the % hybridization signal against days of treatment. The radiograph signal was normalized against the fluorescence signal. Errors denote the standard deviation from three different experiments.

of the G-overhang degradation appeared to vary, with compounds **10** and **17** being the most potent to induce an early effect, a result that is in apparent contrast with their kinetics of cell growth arrest (Fig. 4).

These data suggest that these compounds trigger a telomeric dysfunction associated with the induction of a phenotype reminiscent of cellular senescence. However, the correlation between telomere dysfunction and long-term growth arrest for compounds **9–10**, **15**, **17** and **33** is complex and suggests that additional events contribute to the growth inhibition and the induction of senescence.

Discussion

We have shown that *N*,*N*′-bis(quinolinyl)pyridine-2,6-dicarboxamides in general stabilize G-quadruplex nucleic acids selectively as compared to ds-DNA. Systematic changes of the side chains can help modulate their *in vitro* stabilization potential for G-quadruplexes and differentially affect short- and long-term cell growth. Moreover, their low molecular weight and global structural features confer drug-like properties. This constitutes a promising starting point for the development of compounds with differential growth inhibitory properties on different cell types combined with low toxicity.

The synthesis of the library of compounds was efficient and gave moderate to high yields with high purity in 2–7 synthetic steps. In particular, the coupling of quinoline-based building blocks with the pyridine core using Ghosez' reagent was facile and high yielding compared to other coupling strategies. We demonstrated that diverse simple and complex functional features could be introduced before or after the assembly of the main scaffold, which confers additional flexibility to our synthetic scheme. Functionalization *via* click chemistry, to yield molecules **27–33**, was attractive for chain derivatization at a late stage of the synthesis.[60] Molecules of this family have the ability to stabilize G-quadruplexes formed by the H-Telo sequence in the presence of an excess of ds-DNA (Fig. 2) and also a selection of promoter quadruplexes (Fig. S2 and Table S1†) with very high ΔT_m values, demonstrating the versatility of this type of scaffold to bind G-quadruplex motifs with varying loop sequence. This unique property as a potent generic G-quadruplex binder rationalizes in part the ability of these compounds to target other genomic locations containing putative G-quadruplex forming motifs and to promote genomic instability at well defined genomic locations.[23,58]

The nature of the substitution at the pyridine moiety had a great influence on the stabilization potential of the molecules for H-Telo following the general trend of: amine > Cl > sugar > H > alkoxy. Positively charged functionalities and sugars conferred higher stabilization, most likely due to their potential for electrostatic and hydrogen bonding interactions with the nucleic acid target. Accordingly, substitution with uncharged, aromatic or aliphatic side chains generally had an adverse effect on the stabilization potential of the molecule, which could be due to electronic repulsion or steric clash. Modifications in the length of the side chain linked to the quinoline moiety had a less striking effect, but generally stabilization was higher for chain lengths of three carbons over two carbons. Notably, the stabilization potential for G-quadruplexes was almost eliminated for **14** with methoxy-substitutions on both R^1 and R^2. This shows that the side chains play a crucial role in the potential of the molecules to stabilize G-quadruplex nucleic acids. Clearly, the nature of side chains affected the water solubility properties of each analogue and may reflect differences observed in biophysical and biological assays.

Most of the molecules showed high nanomolar to low micromolar IC_{50}-values for short-term (72 h) growth inhibition against the four cell lines investigated. Some of the compounds, in particular pyridostatin (**1**), **17**, **24**, and **27**, showed a considerable difference in their growth-inhibitory properties between the different cell-lines investigated. Molecules **17**, **24** and **27** were found to be more potent for cancer cell lines over WI-38. Compounds **17** and **24** are more selective towards the cancer cell lines than other analogues that carry a hydrogen or chlorine at position R^1. This shows how the variation of the substitution at R^2 can be used to modulate differential growth inhibitory properties from one cell line to another, which may be exploited further to develop small molecules empowered with selective anti-proliferative properties.

Long-term growth studies upon incubation with the compounds showed that some compounds caused a decrease in population doublings between 6 and 30 days treatment (Fig. 4). In this set of experiments each compound was screened at its IC_{50} value in order to detect and quantify a phenotype, thus enabling a comparative analysis of the analogues. The six compounds with the greatest differential effect on long-term growth were either substituted with an amine side chain (**1**, **9–10**), a chlorine (**15** and **17**) or a sugar at position R^1 (compound **33**).

Consistent with this, these compounds also exhibited very good stabilization of the telomeric quadruplex. None of the molecules substituted with a hydrogen at position R^1 showed a considerable decrease in population doublings upon long-term exposure. Interestingly, all 6 analogues have either a primary amine or a pyrrolidine on the side chain at R^2. The majority of the compounds that induced long-term growth arrest had a side-chain linked by two carbons (with the exception of compound **33**). The cellular growth data suggests an important sensitivity to the R^2 substitution. Compounds **16**, **19** and **22–24** exhibit good short-term growth inhibition, rather than long-term growth effects, which suggest a distinction in biological mechanism(s). Potent stabilization of non-telomeric G-quadruplex structures by FRET-melting (Fig. S2 and Table S1†) may hint that non-telomeric G-quadruplex targeting is the predominant contributing factor to the observed short-term growth arrests. Indeed, our previous reports[23,58] have shown that pyridostatin (**1**) induces DNA damage at non-telomeric *loci* of genomic DNA, resulting in the activation of a cell cycle checkpoint-dependent growth arrest.

Other G-quadruplex ligands have been shown to stabilize telomeric quadruplexes in human cells and cause telomere dysfunction and shortening leading to replicative senescence in telomerase-positive[47] and alternative lengthening of telomeres (ALT)[63,64] cells. Our investigation of the effect of some analogues (**9**–**10**, **15**, **17** and **33**) on the telomeric G-overhang revealed that these derivatives also trigger a telomere dysfunction in HT1080 cells, in agreement with our previous finding that pyridostatin competes for binding at telomeres with the G-overhang binding protein POT1 in HT1080 cells.[23] However, the kinetics for long-term growth inhibition and G-overhang degradation largely differ between these compounds and suggest additional cellular mechanisms. Interestingly, all these derivatives induced senescence during long-term treatments (Fig. S4†) but did not induce an elevated level of cell death, suggesting a mechanism of action different from agents that cause a massive and global DNA damage response throughout the genome. This is in agreement with the targeting properties of *N*,*N*′-bis(quinolinyl)pyridine-2,6-dicarboxamides towards G-quadruplexes. Evidence indicates that telomere dysfunction is one of the causes underpinning cellular senescence.[65] Therefore, the protracted accumulation of DNA damage at telomeres using low concentrations of chemotherapeutic agents to induce accelerated senescence is an increasingly known and investigated mechanism to inhibit tumor cell growth renewal.[66] Thus, long-term growth arrests and senescence induced by these derivatives are noteworthy results of a complex interplay between telomeric effects and the accumulation of restricted DNA damage sites being generated throughout the genome *via* non-telomeric G-quadruplex targeting.

Conclusions

Small molecules with the ability to target telomeres are highly desirable for the treatment of malignant neoplasia, since one of the hallmark of cancer has been defined by the infinite proliferative capacity of cells permitted by mechanisms that sustain telomere length in addition to the ectopic expression of oncogenes.[67] In general, most of the *N*,*N*′-bis(quinolinyl)pyridine-2,6-dicarboxamides that featured in our study showed excellent stabilization of the telomeric G-quadruplex combined with high selectivity over double-stranded DNA, making them suitable chemical agents to target telomeres. The compounds show some striking growth-inhibitory effects on cancer cell-lines after few days of exposure, some of them exhibiting a complete arrest after long-term exposure to the drug. The differential short and long-term inhibitory properties of the different analogues highlights the fact that subtle structural and functional chemical variations of the ligands can be exploited to fine-tune the biological activity of these analogues. Our data are in agreement with a model where both telomeric dysfunction and the accumulation of DNA damage sites at genomic *loci* enriched in G-quadruplex structures trigger a reduced cell growth associated with senescence induction. The selective targeting of G-quadruplexes by *N*,*N*′-bis(quinolinyl)pyridine-2,6-dicarboxamides constitute a promising angle for the development of novel anticancer drugs that could act by impairing cancer mechanisms such as telomere maintenance.

Experimental

FRET-melting studies

100 μM stock solutions of oligonucleotides were prepared in molecular biology grade DNase-free water. Further dilutions were carried out in 60 mM potassium cacodylate buffer, pH 7.4. FRET experiments were carried out with a 200 nM oligonucleotide concentration. All labeled DNA oligonucleotides were supplied by Eurogentec® Ltd and all unlabeled oligonucleotides were supplied by IBA® GmbH. Seven dual fluorescently labeled DNA oligonucleotides were used in these experiments: H-Telo (5′-FAM-GGG TTA GGG TTA GGG TTA GGG-TAMRA-3′), C-kit1 (5′-FAM-GGG AGG GCG CTG GGA GGA GGG-TAMRA-3′), C-kit2 (5′-FAM-GGG CGG GCG CGA GGG AGG GG-TAMRA-3′), C-myc (5′-FAM-TGA GGG TGG GTA GGG TGG GTA A-TAMRA-3′), Bcl-2 (5′-FAM GGG CGC GGG ACG AGG GGG GCG GG-TAMRA-3′), KRAS (5′-FAM AGG GCG GTG TGG GAA GAG GGA AGA GGG GGA GG-TAMRA-3′), ds-DNA (5′-FAM-TAT AGC TAT A-HEG-T ATA GCT ATA-TAMRA-3′) which is a dual-labeled 20-*mer* oligonucleotide comprising a self-complementary sequence with a central polyethylene glycol linker able to fold into a hairpin. The competitor was an unlabeled 26-*mer* oligonucleotide (5′-CAA TCG GAT CGA ATT CGA TCC GAT TG-3′). The donor fluorophore was 6-carboxyfluorescein (FAM) and the acceptor fluorophore was 6-carboxytetramethylrhodamine (TAMRA). The dual-labeled oligonucleotides were annealed at a concentration of 400 nM by heating at 94 °C for 10 min followed by slow cooling to rt at a controlled rate of 0.1 °C min^{-1}. 96-well plates were prepared by addition of 50 μl of the annealed DNA solution to each well, followed by 50 μl solution of molecules **1**, **8–33** at the appropriate concentration. For the competition experiments, competitor was added to the fluorescently labeled quadruplex oligonucleotides sequences at an excess of 50 mol equiv. and annealed in the same solution. Measurements were made in triplicate with an excitation wavelength of 483 nm and a detection wavelength of 533 nm. Final analysis of the data

was carried out using OriginPro 7.5 data analysis and graphing software (OriginLab®).

Cell culture

HeLa, HT1080, U2OS and WI-38 cells were cultured in T-75 flasks in Dulbecco's Modified Eagle's Medium (DMEM) supplemented with 10% fetal calf serum and split at 70–80% confluency using trypsin EDTA. The HT1080, WI-38 and U2OS cells were obtained from the European Collection of Cell Cultures (ECACC) and the HeLa cells were a generous gift of Prof. Ashok Venkitaraman/Cambridge.

Luminescent cell viability assay

IC_{50} values of growth inhibition were determined using the cell viability assay CellTiter-Glo™ (Promega®). Cells were plated in 96 well plates at a density of 4000 cells per well in 100 µl of media and incubated for 24 h. Compounds **1**, **8–33** were added in serial dilutions (in a range between 0–40 µM) at a volume of 100 µl per well at the respective concentrations. Cell viability was measured after 72 h using the manufacturer's protocol. Measurements were taken after 20 min incubation at rt. All measurements were made in triplicate. Final analysis of the data was carried out using OriginPro 7.5 data analysis and graphing software (OriginLab®).

Long-term growth assay and cytotoxicity

HT1080 cells were cultured in T-25 flasks as stated above and seeded at 300 000 cells per flask initially and incubated with **1**, **9–10**, **15–17**, **19–24**, **26–27** and **33** at their respective IC_{50} values or no compound as a control. The cells were split after 3 or 4 days, counted with a hemicytometer and reseeded at their initial density of 300 000 cells per flask. This procedure was repeated every third day. All experiments were performed in triplicate. Population doubling (PD) was calculated using the following formula: PD = $(\ln(n_1/n_2)/\ln 2)$, n_1 = initial number of cells, n_2 = final number of cells. Cytotoxicity was assessed at each time point using a Trypan blue exclusion assay. Cells were counted (as stated above) in a 1 : 1 mixture of media : Trypan blue (0.4% in DMSO). Dead cells were assessed by blue nuclear staining.

β-Galactosidase assay

Senescence was assessed using a senescence β-galactosidase staining kit (Cell Signalling Technology®) according to the manufacturer's protocol. HT1080 cells were cultured in T-75 flasks for 1 d and incubated with compounds **9**, **10**, **15**, **17** and **33** at their respective IC_{50} values for 4 d. As a control, cells were incubated without compound under the same conditions. Cells were split and seeded at 4000 cells per well on a Cover Well™ microscopy slide chamber (Invitrogen®) and incubated with compounds **9**, **10**, **15**, **17** and **33** at the aforementioned concentrations or in the absence of compound for another 4 d. Subsequently, the media was removed and the wells washed twice with 1 × phosphate buffered saline (PBS). Cells were fixed with 2% formaldehyde and 0.2% glutaraldehyde in 1 × PBS for 15 min. This solution was then removed and the wells washed twice with 1 × PBS. Each well was incubated with 800 µl staining solution (40 mM citric acid/sodium phosphate (pH 6.0), 0.15 M NaCl, 2 mM $MgCl_2$, 5 mM potassium ferrocyanide, 5 mM potassium ferricyanide, 1 mg ml^{-1} X-gal, 5% dimethylformamide (DMF)) at 37 °C for 16 h. The staining solution was removed and the cells stored in 70% glycerol.

Non-denaturing hybridization assay

We performed a non-denaturing hybridization assay to detect the 3′ G-overhang. 5 µg of undigested genomic DNA, extracted from cells treated with **9**, **10**, **15**, **17**, **33** or no compound at the respective time points, were hybridized for 16 h at 50 °C with 0.5 pmol of [γ-^{32}P] adenosine triphosphate (ATP)-labeled 21C oligonucleotide (5′-$(CCCTAA)_3CCC$-3′) in 30 µl hybridization buffer (20 mM tris(hydroxymethyl)aminomethane (TRIS)·HCl (pH 8.0), 0.5 mM EDTA, 50 mM NaCl, 10 mM $MgCl_2$). Reactions were stopped by the addition of 9 µl loading buffer (20% glycerol, 1 mM ethylenediaminetetraacetate (EDTA), 0.2% bromophenol blue) and size-fractioned on a 0.7% agarose gel for 3 h at 45 V. The gels were subsequently stained with ethidium bromide (EtBr). The bottom of the gel was cut to remove unbound probe and thus increase resolution. Gels were dried on Whatman® filter paper at 60 °C and exposed overnight on an autoradiography film. Ethidium bromide fluorescence and the autoradiography film were scanned with a phosphorimager (Typhoon™ 9210, Amersham Biosciences®). Results were expressed as the relative hybridization signal normalized to the fluorescent signal of EtBr.

Alphabetical list of non-standard abbreviations

ALT	alternative lengthening of telomeres
ATP	adenosine triphosphate
ATRX	alpha thalassemia/mental retardation syndrome X-linked
Boc	Di-*tert*-butyl dicarbonate
DIAD	diisopropyl azodicarboxylate
DCM	dichloromethane
DMEM	Dulbecco's modified Eagle medium
DMF	*N*,*N*-dimethylformamide
ds-DNA	double stranded DNA
EDTA	ethylenediaminetetraacetic acid
ESI	electrospray ionization
EtBr	ethidium bromide
FAM	6-carboxyfluorescein
FC	flash chromatography
FRET	Förster resonance energy transfer
HPLC	high performance liquid chromatography
IC_{50}	half maximal inhibitory concentration
MeOH	methanol
NaOH	sodium hydroxide
NMR	nuclear magnetic resonance
PD	population doubling
PBS	phosphate buffered saline
POT1	protection of telomeres 1

TAMRA	6-carboxytetramethylrhodamine
TERRA	telomeric repeat containing RNA
TFA	trifluoroacetic acid
THF	tetrahydrofuran
TEBP	telomeric end-binding protein
TLC	thin layer chromatography
T_m	melting temperature
TRF1/2	telometic repeat factor 1/2
TRIS	tris(hydroxymethyl)aminomethane

Acknowledgements

We thank Cancer Research UK for programme funding and for a studentship (S.M.), MUIR FIRB-Ideas RBID082ATK for programme funding (M.D.A.), Ligue Nationale Contre le Cancer for programme funding (J.F.R.), Helen Lightfoot for technical assistance, and Chris Lowe for carefully proofreading this manuscript.

Notes and references

1 I. Bang, *Z. Physiol. Chem.*, 1901, **32**, 201.
2 J. T. Davis, *Angew. Chem., Int. Ed.*, 2004, **43**, 668.
3 M. Gellert, M. N. Lipsett and D. R. Davies, *Proc. Natl. Acad. Sci. U. S. A.*, 1962, **48**, 2013.
4 S. B. Zimmerman, G. H. Cohen and D. R. Davies, *J. Mol. Biol.*, 1975, **92**, 181.
5 I. Cheung, M. Schertzer, A. Rose and P. M. Lansdorp, *Nat. Genet.*, 2002, **31**, 405.
6 L. Cahoon and H. S. Seifert, *Science*, 2009, **325**, 764.
7 P. Sarkies, C. Reams, L. J. Simpson and J. E. Sale, *Mol. Cell*, 2010, **40**, 703.
8 K. Paeschke, J. A. Capra and V. A. Zakian, *Cell*, 2011, **145**, 678.
9 K. Paeschke, T. Simonsson, J. Postberg, D. Rhodes and H. J. Lipps, *Nat. Struct. Mol. Biol.*, 2005, **12**, 847.
10 R. K. Moyzis, J. M. Buckingham, L. S. Cram, M. Dani, L. Deaven, M. D. Jones, J. Meyne, R. L. Ratliff and J. R. Wu, *Proc. Natl. Acad. Sci. U. S. A.*, 1988, **85**, 6622.
11 G. N. Parkinson, M. P. H. Lee and S. Neidle, *Nature*, 2002, **417**, 876.
12 Y. Wang and D. J. Patel, *J. Mol. Biol.*, 1993, **234**, 1171.
13 D. Sun, B. Thompson, B. E. Cathers, M. Salazar, S. M. Kerwin, J. O. Trent, T. C. Jenkins, S. Neidle and L. H. Hurley, *J. Med. Chem.*, 1997, **40**, 2113.
14 D. Gomez, T. Wenner, B. Brassart, C. Douarre, M.-F. O'Donohue, V. E. Khoury, K. Shin-ya, H. Morjani, C. Trentesaux and J.-F. Riou, *J. Biol. Chem.*, 2006, **281**, 38721.
15 A. Rizzo, E. Salvati, M. Purru, C. D'Angelo, M. F. Stevens, M. D'Incalci, C. Leonetti, E. Gilson, G. Zupi and A. Biroccio, *Nucleic Acids Res.*, 2009, **37**, 5353.
16 C. M. Azzalin, P. Reichenbach, L. Khoriauli, E. Giulotto and J. Lingner, *Science*, 2007, **318**, 798.
17 A. M. Zahler, J. R. Williamson, T. R. Cech and D. M. Prescott, *Nature*, 1991, **350**, 718.
18 D. J. Bearss, L. H. Hurley and D. D. V. Hoff, *Oncogene*, 2000, **19**, 6632.
19 S. Neidle and G. Parkinson, *Nat. Rev. Drug Discovery*, 2002, **1**, 383.
20 A. D. Cian, G. Cristofari, P. Reichebach, E. D. Lemos, D. Monchaud, M.-P. Teulade-Fichou, K. Shin-ya, L. Lacroix, J. Lingner and J.-L. Mergny, *Proc. Natl. Acad. Sci. U. S. A.*, 2007, **104**, 17347.
21 D. Gomez, A. Guédin, J. L. Mergny, B. Salles, J.-F. Riou, M.-P. Teulade-Fichou and P. Calsou, *Nucleic Acids Res.*, 2010, **20**, 7187.
22 T. de Lange, *Genes Dev.*, 2005, **19**, 2100.
23 R. Rodriguez, S. Müller, J. A. Yeoman, C. Trentesaux and J.-F. Riou, *J. Am. Chem. Soc.*, 2008, **130**, 15758.
24 F. d'Adda di Fagagna, P. M. Reaper, L. Clay-Ferrace, H. Flegler, P. Carr, T. von Zglinicki, G. Saretzki, N. P. Carter and S. P. Jackson, *Nature*, 2005, **426**, 194.
25 J. L. Huppert and S. Balasubramanian, *Nucleic Acids Res.*, 2005, **33**, 2908.
26 J. L. Huppert and S. Balasubramanian, *Nucleic Acids Res.*, 2007, **35**, 406.
27 H. Fernando, A. P. Reszka, J. Huppert, S. Ladame, S. Rankin, A. R. Venkitaraman, S. Neidle and S. Balasubramanian, *Biochemistry*, 2006, **45**, 7854.
28 S. Rankin, A. P. Reszka, J. Huppert, M. Zloh, G. N. Parkinson, A. K. Todd, S. Ladame, S. Balasubramanian and S. Neidle, *J. Am. Chem. Soc.*, 2005, **127**, 10584.
29 A. T. Phan, Y. S. Modi and D. J. Patel, *J. Am. Chem. Soc.*, 2004, **126**, 8710.
30 A. Siddiqui-Jain, C. Grand, D. J. Bearss and L. H. Hurley, *Proc. Natl. Acad. Sci. U. S. A.*, 2002, **99**, 11593.
31 J. Dai, D. Chen, R. A. Jones, L. H. Hurley and D. Yang, *Nucleic Acids Res.*, 2006, **34**, 5133.
32 S. Cogoi and L. E. Xodo, *Nucleic Acids Res.*, 2006, **34**, 2536.
33 M. Bejugam, M. Gunaratnam, S. Müller, D. A. Sanders, S. Sewitz, J. A. Fletcher, S. Neidle and S. Balasubramanian, *ACS Med. Chem. Lett.*, 2010, **1**, 306.
34 M. Bejugam, S. Sewitz, P. S. Shirude, R. Rodriguez, R. Shahid and S. Balasubramanian, *J. Am. Chem. Soc.*, 2007, **129**, 12926.
35 S. Kumari, A. Bugaut, J. L. Huppert and S. Balasubramanian, *Nat. Chem. Biol.*, 2007, **3**, 218.
36 D. J. Patel, A. T. Phan and V. Kuryavyi, *Nucleic Acids Res.*, 2007, **35**, 7429.
37 C. Schaeffer, B. Bardoni, J.-L. Mandel and B. Ehresmann, *EMBO J.*, 2001, **20**, 4803.
38 A. Bugaut, R. Rodriguez, S. Kumari, S.-T. Hsu and S. Balasubramanian, *Org. Biomol. Chem.*, 2010, **8**, 2771.
39 D. Gomez, T. Lemarteleur, L. Lacroix, P. Mailliet, J.-L. Mergny and J.-F. Riou, *Nucleic Acids Res.*, 2004, **32**, 371.
40 M. J. Law, K. M. Lower, H. P. J. Voon, J. R. Hughes, D. Garrick, V. Viprajasit, M. Mitson, M. D. Gobbi, M. Marra, A. Morris, A. Abbott, S. P. Wilder, S. Taylor, G. M. Santos, J. Cross, H. Ayyub, S. Jones, J. Ragoussis, D. Rhodes, I. Dunham, D. R. Higgs and J. R. Gibbons, *Cell*, 2010, **143**, 367.
41 M. Di Antonio, F. Doria, S. N. Richter, C. Bertipaglia, M. Mella, C. Sissi, M. Palumbo and M. Freccero, *J. Am. Chem. Soc.*, 2009, **131**, 13132.
42 W. C. Drewe, R. Nanjunda, M. Gunaratnam, M. Beltran, G. N. Parkinson, A. P. Reszka, W. D. Wilson and S. Neidle, *J. Med. Chem.*, 2008, **51**, 7751.
43 K. Jantos, R. Rodriguez, S. Ladame, P. S. Shirude and S. Balasubramanian, *J. Am. Chem. Soc.*, 2006, **128**, 13662.
44 M. Y. Kim, H. Venkayalapati, K. Shin-Ya, K. Wierzba and L. H. Hurley, *J. Am. Chem. Soc.*, 2002, **124**, 2098.
45 C. Leonetti, S. Amodei, C. D'Angelo, A. Rizzo, B. Banassi, A. Antonelli, R. Elli, M. F. Stevens, M. D'Incalci, G. Zupi and A. Biroccio, *Mol. Pharmacol.*, 2004, **66**, 1138.
46 M. J. B. Moore, C. M. Schulters, J. Cuesta, F. Cuenca, M. Gunaratnam, F. A. Tanious, W. D. Wilson and S. Neidle, *J. Med. Chem.*, 2006, **49**, 582.
47 J.-F. Riou, L. Guittat, P. Mailliet, A. Laoui, E. Renou, O. Petitgenet, F. Mégnin-Chanet, C. Hélène and J.-L. Mergny, *Proc. Natl. Acad. Sci. U. S. A.*, 2002, **99**, 2672.
48 R. Rodriguez, G. D. Pantoş, D. P. N. Gonçalves, J. K. M. Sanders and S. Balasubramanian, *Angew. Chem., Int. Ed.*, 2007, **46**, 5404.
49 J.-H. Tan, T.-M. Ou, J.-Q. Hou, Y.-J. Lu, S.-L. Huang, H.-B. Luo, J.-Y. Wu, Z.-S. Huang, K.-Y. Wong and L.-Q. Gu, *J. Med. Chem.*, 2009, **52**, 2825.
50 Z. A. E. Waller, P. S. Shirude, R. Rodriguez and S. Balasubramanian, *Chem. Commun.*, 2008, 1467.
51 A. D. Cian, E. DeLemos, J.-L. Mergny, M.-P. Teulade-Fichou and D. Monchaud, *J. Am. Chem. Soc.*, 2007, **129**, 1856.
52 C. Granotier, G. Pennarun, L. Riou, F. Hoffschir, L. R. Gauthier, A. D. Cian, D. Gomez, E. Mandine, J.-F. Riou, J.-L. Mergny, P. Mailliet, B. Dutrillaux and F. D. Boussin, *Nucleic Acids Res.*, 2005, **33**, 4182.
53 S. Müller, G. D. Pantoş, R. Rodriguez and S. Balasubramanian, *Chem. Commun.*, 2009, 80.
54 P. S. Shirude, E. R. Gillies, S. Ladame, F. Godde, K. Shin-Ya, I. Huc and S. Balasubramanian, *J. Am. Chem. Soc.*, 2007, **129**, 11890.
55 S. L. Jain, P. Bhattacharyya, H. L. Milton, A. M. Z. Slawin, J. A. Crayston and J. D. Woollins, *Dalton Trans.*, 2004, 862.
56 S. Müller, S. Kumari, R. Rodriguez and S. Balasubramanian, *Nat. Chem.*, 2010, **2**, 1095.
57 D. Koirala, S. Dhakal, B. Ashbridge, Y. Sannohe, R. Rodriguez, H. Sugiyama, S. Balasubramanian and H. Mao, *Nat. Chem.*, 2011, **3**, 782.
58 R. Rodriguez, K. M. Miller, J. V. Forment, C. R. Bradshaw, M. Nikan, S. Britton, T. Oelschlaegel, B. Xhemalce, S. Balasubramanian and S. P. Jackson, *Nat. Chem. Biol.*, 2011, **8**, 301.

59 J.-L. Mergny and J.-C. Maurizot, *ChemBioChem*, 2001, **2**, 124.
60 V. V. Rostovtsev, L. G. Green, V. V. Fokin and K. B. Sharpless, *Angew. Chem., Int. Ed.*, 2002, **41**, 2596.
61 P. Auffinger, F. A. Hays, E. Westhof and P. S. Ho, *Proc. Natl. Acad. Sci. U. S. A.*, 2004, **48**, 16789.
62 D. Gomez, R. Paterski, T. Lemarteleur, K. Shin-Ya, J. L. Mergny and J.-F. Riou, *J. Biol. Chem.*, 2004, **279**, 41487.
63 A. J. Cesare and R. R. Reddel, *Nat. Rev. Genet.*, 2010, **11**, 319.
64 N. Temime-Smaali, L. Guittat, A. Sidibe, K. Shin-ya, C. Trentesaux and J.-F. Riou, *PLoS One*, 2009, **4**, 6919.
65 F. d'Adda di Fagagna, *Nat. Rev. Cancer*, 2008, **8**, 512.
66 D. A. Gewirtz, S. E. Holt and L. W. Elmore, *Biochem. Pharmacol.*, 2008, **76**, 947.
67 D. Hanahan and R. Weinberg, *Cell*, 2011, **144**, 646.

